Elucidation of local structure deformation in κ-(BEDT-TTF)$_2$Cu[N(CN)$_2$]Br by x-ray fluorescence holography

Artoni Kevin R. Ang ●,[1,*] Riho Marumi,[1] Ayana Sato-Tomita ●,[2] Koji Kimura,[1] Naohisa Happo,[3] Kazuto Akagi,[4] Takahiko Sasaki ●,[5] and Kouichi Hayashi[1,6]

[1]*Department of Physical Science and Engineering, Nagoya Institute of Technology, Gokiso, Showa, Nagoya 466–8555, Japan*

[2]*Division of Biophysics, Department of Physiology, Jichi Medical University, Yakushiji, Shimotsuke, Tochigi 329–0498, Japan*

[3]*Department of Computer and Network Engineering, Graduate School of Information Sciences, Hiroshima City University, Asa Minami-ku, Hiroshima 731–3194, Japan*

[4]*Advanced Institute for Materials Research (AIMR), Tohoku University, 2-1-1 Katahira, Aoba, Sendai 980–8577, Japan*

[5]*Institute for Materials Research, Tohoku University, 2-1-1 Katahira, Aoba, Sendai 980–8577, Japan*

[6]*Frontier Research Institute for Materials Science, Nagoya Institute of Technology, Gokiso, Showa, Nagoya 466–8555, Japan*

κ-(BEDT-TTF)$_2$Cu[N(CN)$_2$]Br (κ-Br) is an organic superconductor that changes to an Anderson-type insulator due to the random defects introduced by x-ray irradiation. In this study, we directly investigated the effects of irradiation on the local structures in the anion layer of κ-Br using x-ray fluorescence holography. The local structures around the Cu atoms in the anion layer were directly reconstructed from holograms. Prior to radiation damage, the reconstruction clearly shows the atomic images of the Br and N atoms that are directly coordinated to Cu. In the irradiated samples, the N images in the reconstructions were strongly suppressed as a result of the positional fluctuations of N introduced by the defects induced by irradiation. Using the previously proposed "bond-shifted" model and the thermal vibration amplitudes calculated from molecular dynamics simulations, we simulated the holograms and the atomic reconstructions of the anion layer. The simulations show that the "bond-shifted" model, along with thermal vibrations at 100 K, suppresses the N atomic images, as was observed in the experimental reconstructions.

I. INTRODUCTION

κ-(BEDT-TTF)$_2$Cu[N(CN)$_2$]Br (κ-Br) is an organic charge transfer salt based on the donor molecule C$_6$S$_8$[(CH$_2$)$_2$]$_2$ or bis(ethylenedithio)-tetrathiafulvalene (BEDT-TTF). It is one of a general class of κ-(BEDT-TTF)$_2X$, with $X =$ Cu(NCS)$_2$, Cu[N(CN)$_2$]Br, Cu$_2$(CN)$_3$, etc., that have attracted significant attention as strongly correlated π-electron systems [1]. There have been reports that random defects introduced by x-ray irradiation can significantly change the electronic properties of these materials [2–6]. In particular, κ-Br has been reported to change from a superconductor to an Anderson-type localization insulator due to these defects [4]. Contrary to Mott metal-insulator (MI) transitions, where electron localization occurs when the mutual Coulomb repulsion of electrons at the same site, U, exceeds the band width, W, the electron localization in Anderson insulators is due to the interference of the electron wave functions due to the disorder in the system. This disorder is introduced into κ-Br by the formation of random defects after x-ray irradiation.

Experimentally, these random defects have not been directly observed in κ-Br. There is a lack of detectable changes in the diffraction images even after long irradiation times. From the infrared optical conductivity spectra, x-ray irradiation showed a suppression of the molecular vibration modes associated with the C–N and C $\equiv$ N bonds of the dicyanamide (DCA) molecules in the anion layer [5,6], suggesting that the radiation damage is limited to the anion layer. First-principles calculations have shown that these deformations can be formed by a "bond-shifted" (BS) model, where the excitation of light elements (C and N) is critical in the deformation process [7]. The BS model is triggered by the breaking of C–N bonds in the DCA molecules. The bond shift occurs when a C $\equiv$ N fragment of a broken DCA$^-$ molecule connects with a N–C $\equiv$ N fragment of the adjacent DCA$^-$ molecule to form a new molecule oriented in a different direction. The calculated vibration spectra indicated that the BS model results in the decrease of the C–N and C $\equiv$ N vibration modes, and the calculated local density of states of the "bond-shifted" anion layer results in electrostatic potential modulations. Such random potential modulation in the anion layer affects the conductive behavior of the π electrons in the BEDT-TTF cation layers, causing the increase in the resistivity of the system even without radiation-induced deformations in the BEDT-TTF molecules themselves [7]. However, there are still no direct experimental verifications for this BS model. Structural information about these local deformations will be beneficial to our understanding of MI transitions, particularly for this class of materials.

The local distortions that produce the BS model does not necessarily have long-range translation symmetry, which

*angartoni.kevinroquero@nitech.ac.jp

makes it difficult to investigate using conventional x-ray based structural determination techniques. X-ray diffraction (XRD), and x-ray absorption fine structure (XAFS) techniques are among some of the most commonly used tools in investigating the structures of materials. However, XRD gives only averaged, long-range translational periodicity, which makes it hard to resolve nonperiodic atomic scale distortions. XAFS, on the other hand, can provide element sensitive, atomic resolution information about the local structures around atoms of a particular element, but this information is limited to a radial angle-integrated one-dimensional distribution of surrounding atoms.

Unlike XRD or XAFS, x-ray fluorescence holography (XFH) is uniquely capable of visualizing the three-dimensional (3D) arrangement of atoms of these nonperiodic local structures [8,9]. XFH is an atomic resolution holography technique that utilizes atoms of a target element in the material as point sources of fluorescent x-rays. The interference between the fluorescent x-rays (reference wave) and the x-rays scattered by the surrounding atoms (object wave) stores the 3D arrangement of these scatterers as a hologram. A 3D reconstruction of this atomic structure can be directly obtained from the holograms by applying reconstruction algorithms, without needing prior structural information about the sample. XFH has been used to reveal the local structures in metal alloys [10], and around dopants in various functional materials [11,12]. XFH has been particularly powerful in imaging atomic scale distortions [13–15]. More detailed discussions about the principles of XFH, and more comprehensive reviews of recent papers have been published elsewhere [9,16].

While XFH has mostly been used on inorganic crystals, work has recently started on adapting XFH for use on soft matter [17,18]. Additional experimental difficulties are introduced in XFH when working with soft matter, these include low metal concentrations, backscattering from the sample holder, and x-ray induced damage on the sample. A successful demonstration of XFH of soft matter was reported in 2016 by some of the authors of this work, where an XFH apparatus designed for protein crystals was developed and tested on a hemoglobin crystal [17]. Using this apparatus, Fe holograms were obtained without inducing radiation damage on the crystal. However, a clear atomic image was not obtained in the reconstruction due to the complicated local structures around the multiple nonequivalent Fe emitters in the hemoglobin heme [17]. A clear reconstruction from the anion layer of pristine κ-Br was partially reported in Ref. [18].

In this paper, a successful XFH experiment on an organic sample is reported. The atomic reconstructions obtained clearly show the Br and N atoms around Cu in the anion planes of the pristine κ-(BEDT-TTF)$_2$Cu[N(CN)$_2$]Br sample. The changes in the local structure of κ-Br upon x-ray irradiation were directly observed by XFH. The N atomic images were suppressed in the reconstruction, a clear indication of radiation damage in the DCA groups. XFH simulations using the pristine model show strong Br and N atomic images, which partially agrees with the experimental results. Simulations using the BS model also show strong Br and N atomic images, which is inconsistent with the strongly suppressed N images in the irradiated samples observed in the experiments. To im-
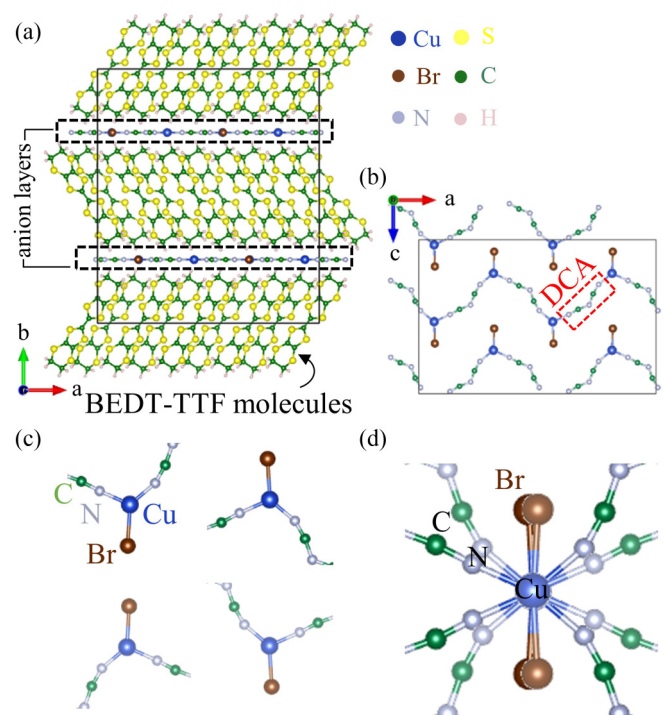

FIG. 1. (a) Structural model of the pristine κ-(BEDT-TTF)$_2$Cu[N(CN)$_2$]Br crystal, (b) the anion layer, (c) the four inequivalent Cu sites in the anion layer and (d) the superposition of local structures centered around the Cu atoms.

prove the simulations, the positional fluctuations from thermal vibrations were calculated from molecular dynamics (MD) simulations, and used in the hologram simulations. Simulations at 100 K showed that the increased dynamic fluctuations in the relative positions of the N atoms can introduce strong suppressions of the N atomic images. The simulations at 100 K for both the pristine and BS model showed good agreement with the experiment, suggesting the BS model is a good approximation of the defects introduced by x-ray irradiation. These results show the unique capabilities of XFH in investigating the local structures around metal atoms in soft-matter, opening up the possibilities for future bio-XFH experiments.

II. EXPERIMENT AND COMPUTATIONAL DETAILS

A. κ-Br crystal preparation

The κ-Br single crystals were prepared and irradiated with x-rays as described in Ref. [4]. The crystals were grown using a standard electrochemical oxidation method, and were irradiated at 300 K using a nonfiltered tungsten target at 40 kV and 20 mA, at a dose rate of 0.5 MGy/h [2,3].

Figure 1(a) shows the orthorhombic crystal structure of the κ-Br crystal, with space group *Pnma* and lattice parameters $a = 12.884(5)$ Å, $b = 29.581(8)$ Å and $c = 8.484(4)$ Å at 100 K [19]. This organic charge-transfer salt is based on the donor molecule BEDT-TTF, with the anion layer consisting of Cu[N(CN)$_2$]Br [Fig. 1(b)]. The anion layers consist of two inequivalent Cu sites each, as shown in Fig. 1(b), and the two anion layers are related by symmetry. All four inequivalent
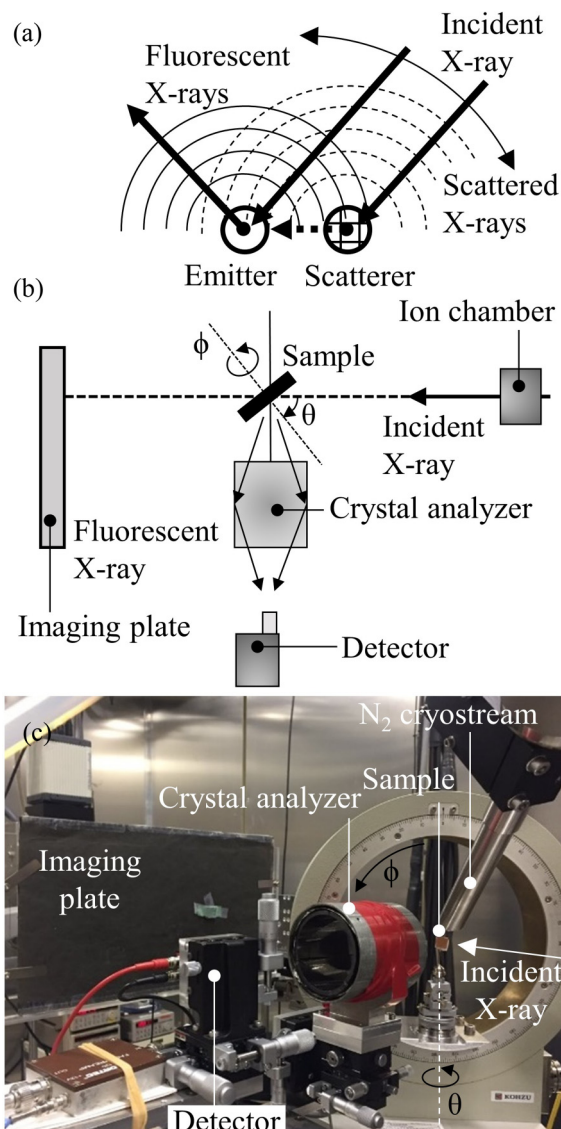
FIG. 2. Schematic diagrams of (a) the inverse mode XFH experiment used in this study, and (b) the experimental setup, (c) photo of the bio XFH apparatus used in BL37XU, SPring-8.

sites in the unit cell are shown in Fig. 1(c), and the superposition of these different local structures are shown in Fig. 1(d).

Three samples were prepared for the XFH experiments: a pristine, nonirradiated sample, and two irradiated samples: a low-dose sample irradiated for 200 h, and a high-dose sample irradiated for 500 h.

B. x-ray fluorescence holography

The local structures in κ-Br were investigated using inverse-mode XFH. The XFH apparatus developed for protein crystals in Ref. [17] was used in this experiment. The principles behind inverse-mode XFH, and a schematic diagram of the XFH experiment is shown in Fig. 2.

To address the unique challenges soft matter pose on XFH, the fluorescent x-rays were focused using a graphite crystal analyzer on an avalanche photodiode, a special sample holder was used to minimize backscattering, the incident x-ray flux

was controlled, and the sample was cooled to 100 K using a liquid nitrogen gas flow system to minimize additional radiation damage during the experiment [17]. Diffraction patterns were taken immediately before and after the XFH experiments to monitor for any radiation damage [20]. The in-plane resistivities were also measured after the experiment to check for additional radiation damage [20].

The XFH experiments were performed in BL37XU and BL39XU of SPring-8, Japan. The experiments were done using a $10 \times 25\,\mu m^2$ x-ray beam focused using a Kirkpatrick-Baez mirror. The photon flux was set by variable Al film attenuators to $\sim 10^9$ photons/s. The Cu-Kα holograms were recorded using incident x-ray energies of $9.5-12.0$ keV, at intervals of 0.5 keV. The angular scan ranges were: $0–75°$ for the polar angle θ and $0–360°$ for the azimuthal angle ϕ. For each incident x-ray energy, the hologram scan took ~ 3 h, resulting in an average dose of ~ 3 MGy for each sample [21]. The experiment and the data processing have been discussed in detail elsewhere [9,17,18]. To extend the experimental holograms, symmetry operations were applied: twofold symmetry along the x, y, and z axis, and mirror planes in the xy, yz, and xz planes. The simulated holograms were masked to the same size as the experimental hologram and the same symmetry operations were also applied. The 3D atomic images were reconstructed from the experimental and simulated holograms using Barton's algorithm [22]. Details of the sample preparation and XFH experiments are summarized in Table I.

C. Calculation details

The structure optimization and molecular dynamics calculations were done using the Vienna *ab initio* simulation package [23] with the revised van der Waals–density functional (vdW-DF2) [24], which can reproduce vdW interaction. The projector-augmented-wave scheme was used with the plane-wave cutoff energy of 500 eV and Γ-point sampling. While 2×2 size unit cell was used for the pristine and bond shift model, 1×4 size unit cell was used for the bond breaking model. After both the atomic configurations and the lattice parameters were optimized for each system, MD simulation with NVT ensemble at 100 and 300 K were performed. The time step was 1.0 fs (the mass of hydrogen atoms was 2.0).

III. RESULTS AND DISCUSSION

A. Pristine κ-Br crystals

Using a 50-Å radius cluster built using the pristine κ-Br structural model shown in Fig. 1(a), x-ray fluorescence holograms were calculated using the same incident x-ray energies as the experimental holograms. Furthermore, the as-simulated holograms were rotated and masked to match the scanned region in the experimental holograms. The simulated and experimental holograms with an incident x-ray energy of 11.0 keV are shown in Fig. 3 after application of a low pass filter. The Cu Kα fluorescent intensities recorded were in the same order as typical XFH experiments reported. The prominent feature in the simulated hologram is the curved lines marked by the white dashed line in Fig. 3(a), and appear to be x-ray standing wave (XSW) lines. Typical holograms from

TABLE I. Details of the sample preparations and XFH experiments for κ-Br.

	Before irradiation	After irradiation	
Irradiation time [4]	-	200h	500h
XFH experiment	BL39XU, SPring-8	BL37XU, SPring-8	BL37XU, SPring-8
Incident x-ray energies	9.5 keV −12.0 keV	9.5 keV −12.0 keV	9.5 keV −12.0 keV
Polar angle θ range	0°−75°	0°−75°	0°−75°
Step size	1 °	1 °	1 °
Azimuthal angle ϕ range	0°−360°	0°−360°	0°−360°
Step size	0.25 °	0.25 °	0.25 °
Fluorescent x-ray	Cu Kα	Cu Kα	Cu Kα
Fluorescent Intensity	4900 counts/degree	2200 counts/degree	2800 counts/degree

inorganic samples are dominated by strong and sharp lines known as Kossel lines or XSW lines, which contain structural information about the long-range order of the sample [16]. Kossel lines are formed when the fluorescent x-rays from an emitter atom in the sample are scattered by lattice planes satisfying the Bragg condition, where strong intensity variations are observed along the cone whose axis is perpendicular to these planes [25,26]. For soft-materials, which are mostly composed of light elements and have large and complicated unit cells, such XSW line features are not expected to be dominant. However, the fine holographic oscillations observed agree with the general features of the holograms recorded from the protein crystal hemoglobin [17]. In the simulation, curved lines (indicated by the white dashed line) appears. This

is also roughly observed in the experiment, even prior to the application of symmetry operations [Fig. 3(b)].

The successful reconstruction of the atomic images from the holograms confirmed that the fluorescence patterns recorded contain the holographic signal. The anion plane was reconstructed from the simulated and experimental holograms of the pristine κ-Br sample using Barton's algorithm [22], and are shown in Fig. 4. The circles overlaid on the left side of the atomic images are the expected atomic positions of the neighboring Br, N, and C atoms extracted from the structural model of pristine κ-Br, as shown in Fig. 4(c).

In the reconstruction from the experimental holograms [Fig. 4(a)], strong atomic image intensities were observed at the Br positions, while weak images were observed at the N
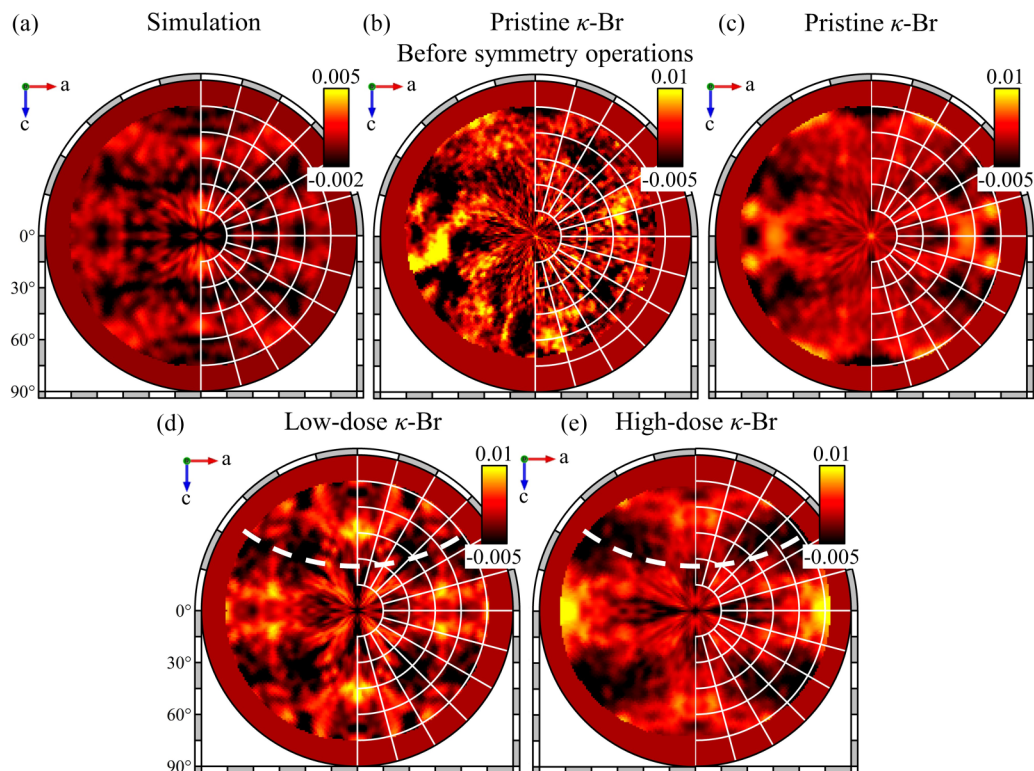

FIG. 3. (a) Cu Kα hologram calculated at an incident x-ray energy of 11.0 keV for a pristine κ-Br crystal, and the experimental Cu Kα holograms taken at 11.0 keV for a pristine κ-Br crystal (b) before and (c) after the application of symmetry operations, and κ-Br crystals irradiated at (c) low dose (200 h), and (d) high dose (500 h). A low pass filter (Gaussian convolution FWHM $\sim$ 3 °) was applied for this figure.
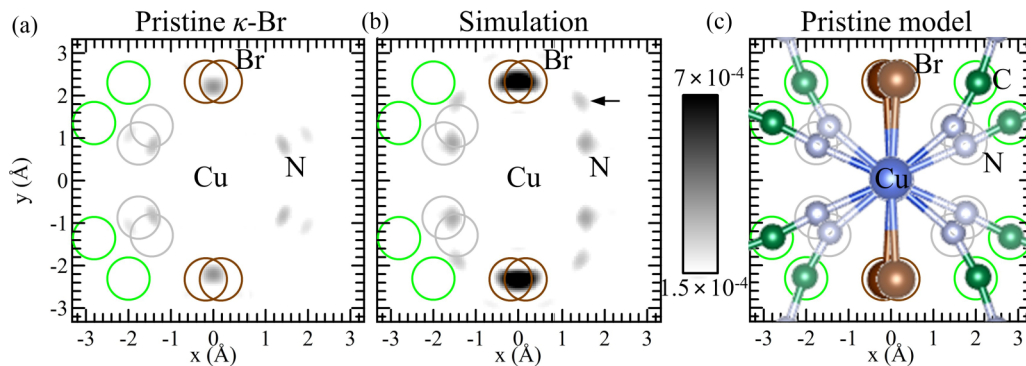
FIG. 4. Atomic images of the anion plane reconstructed from the (a) experimental and (b) simulated Cu Kα holograms from the pristine κ-Br samples, and (c) the superposition of the local structures around Cu atoms in the structural model for the κ-Br sample. The circles represent the ideal positions of atoms around Cu calculated from the structural model of the pristine κ-Br.

positions. Overall, this is in good agreement with the simulation in Fig. 4(b). From these atomic images, the Cu–Br and Cu–N bond lengths were obtained and compared with values obtained from XRD and EXAFS results previously reported in the literature and are shown in Table II.

For both the experiment and the simulations, the N atomic images are shifted towards the Cu emitter, as seen in the reconstructions in Fig. 4, and in the Cu-N bond lengths in Table II. The atomic images in the reconstruction represent the average positions of the surrounding atoms and could result in these small shifts in the atomic position.

Aside from the Br and N atomic images, additional images are also observed between the Br and N positions in the simulations, indicated by the black arrow in Fig. 4(b). This is an artifact that results from the masking of the as-simulated hologram pattern, resulting in truncation error in the reconstruction [20].

In the reconstruction from both the experiment and the simulation, the C atoms in the anion plane are not visible. In general, the atomic image intensity obtained in XFH depends on the x-ray scattering cross section, its distance from the emitter atom, and positional fluctuation of that atom. The x-ray scattering cross section of C and N are much lower than Br, and are expected to produce weak atomic images in the reconstruction. Furthermore, the complicated structure of this sample results in the weak visibility of the atomic images. Light elements are rarely observed in the atomic reconstructions in XFH, even for simpler inorganic crystals. So far, the lightest element observed in XFH is O in the atomic images reconstructed from Pb Lα holograms from Pb(Mn$_{1/3}$Nb$_{2/3}$)O$_3$ [30], and Y Kα holograms from YO sam-

ples [31]. In this work, the appearance of the N atomic images may be due to its proximity to the Cu emitter and the overlap in the N positions in the different local structures, as shown in Fig. 4(c).

These results are the first successful atomic reconstructions from x-ray fluorescence holograms recorded from organic samples. Unlike the hemoglobin crystal used in Ref. [17], the region of interest in this study is limited to the 2D anion layer in the sample, which is much simpler than the complicated arrangement of the heme planes in the hemoglobin unit cell. Furthermore, there are only four inequivalent local structures around Cu, making the interpretation of the reconstruction simpler than, unlike for example, the 16 distinct Fe environments in hemoglobin [17].

B. Radiation induced deformations

To investigate the effects of x-ray irradiation on the local structures of the anion layer of κ-Br, XFH experiments were also performed on irradiated samples. Two irradiated samples were measured for this study, a sample irradiated at low dose (irradiation time, $t^{irr} = 200$ h) and another at high dose ($t^{irr} = 500$ h). These samples were chosen to obtain information across the MI transition. For the pristine samples, the resistivity curve shows a broad hump at 100 K, a crossover from a bad to good metallic state, and finally, the superconducting transition at $T_c = 11$ K [4,32]. For $t^{irr} < 100$ h, x-ray irradiation changes the $\rho(T)$ resistivity behavior of κ-Br, with the residual resistivity, ρ_0, increasing and the superconducting transition temperature T_c decreasing almost linearly with irradiation time [4]. At $t^{irr} = 200$ h, $\rho(T)$ is almost temperature independent before sharply dropping at $T_c \approx 6$ K [4]. At 500 h, the resistivity at 4 K is more than 5 orders of magnitude larger than the pristine κ-Br.

The resistivity curves, $\rho(T)$ and the diffraction images taken after the XFH experiments indicate that no further defects were introduced [20]. The atomic reconstructions of the anion layer are shown in Figs. 5(a) and 5(b).

In the reconstructed atomic images of the both the low- and high-dose samples [Figs. 5(a) and 5(b)], the Br atoms are well reproduced in the reconstructions. The N atomic images, however, could not be observed above the background noise

TABLE II. Summary of the Cu–Br and Cu–N bond lengths of κ-Br.

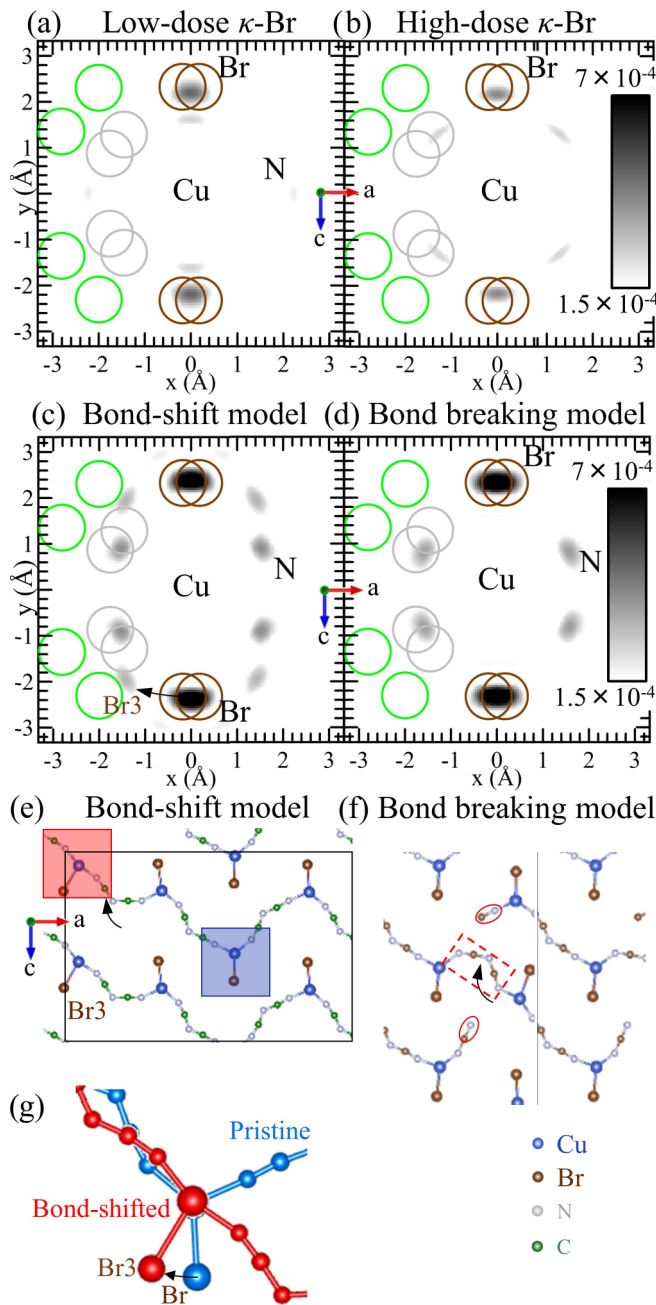|		Cu–Br (Å)	Cu–N (Å)	Temperature (K)
XFH	Exp.	2.20	1.64	100
	Sim.	2.35	1.70	0
XRD	Ref. [27]	2.32	1.95	298
	Ref. [28]	2.33	1.96	127
EXAFS	Ref. [29]	2.32	1.95	100

FIG. 5. Atomic images of the anion plane reconstructed from the experimental Cu Kα holograms recorded from the κ-Br samples irradiated with (a) low dose (200 h) and (b) high dose (500 h) x-rays, from holograms simulated using (c) the "bond-shift" model and (d) the "bond-breaking" model. Structural models of (e) the BS model, (f) the BB model, and (g) a superposition of the pristine and BS models.

levels in the reconstructed images, suggesting that radiation damage results in the suppression of the N atomic image intensities. In XFH, the suppression of the atomic image intensities can generally be attributed to changes in the static or dynamic (thermal vibrations) positional fluctuations between the scatterer and the emitter [33]. However, it is difficult to differentiate the effects of static and dynamic fluctuations in the atomic images. To isolate the effects of static fluctuations,

which consists of the spatial distributions of the atoms around the emitter, the holograms and resulting atomic reconstructions were calculated at 0 K using different structural models proposed for the irradiated κ-Br.

First, the "bond-shift" model proposed in Ref. [7] was considered. In the reconstruction obtained from the hologram simulations using the BS model [Fig. 5(c)], the Br and N atomic images were clearly reproduced, similar to the atomic reconstruction from the pristine κ-Br in Fig. 4(b). However, additional atomic images are also observed. As a result of the bond shifts in the BS model, some Br atoms [labeled Br3 in Fig. 5(e)] are significantly shifted from the Br sites in the pristine model [Fig. 5(d)], resulting in the additional images in the reconstruction [20].

While the atomic images of these shifted Br atoms were well reproduced in the reconstruction [Fig. 5(c)], these were not observed in the experiment, for both the low- and high-dose samples [Figs. 5(a) and 5(b)]. This could be due to the concentration of the bond-shifts in the samples being lower than the 25% defect concentration in the BS model used for the simulations, and thus, the atomic image intensities of these shifted Br atoms are too weak to be observed in the reconstruction. In the calculations of the vibration modes of κ-Br with 0% (pristine) and 25% "bond-shifted" regions, new peaks corresponding to the C–N and C $\equiv$ N vibration modes related to the "bond-shifted" regions were observed [7]. Experimentally, however, these new peaks were not observed [5], suggesting that the irradiated κ-Br samples have lower bond-shift concentrations.

Aside from the atomic images of the shifted Br atoms, strong N atomic images were also observed in the reconstruction, which is contradictory to the missing N atomic images in the experimental reconstructions.

Additional structural models were explored to try and model the experimental results. Several models were prepared and optimized using first-principles calculations. First, an extreme case where all DCA molecules were pivoted was considered, a 100% "bond-shifted" model. Upon structural optimization, the DCA network of this model was unstable and fragmented. In another model considered, random defects were introduced into the anion layer assuming randomly generated core holes at some DCA units, but again, in this model, the DCA networks fragmented during the structural optimization process.

A stable structure was found when only a single defect is introduced in the anion layer. In this scenario, a single C-N bond breaking is introduced in a DCA molecule in the anion layer. This is the single-excitation scenario proposed for the formation of the BS model in Ref. [7]. While the resulting structure was stable after structure optimization even at 300 K, the broken DCA fragment promptly rebonds, and the structure reverts back to an almost pristine k-Br structure.

By introducing a second C-N bond breaking in an adjacent DCA molecule, a single "bond shift" is induced. This is the double-excitation scenario in Ref. [7]. In this model, a N–C $\equiv$ N fragment bonds with the C $\equiv$ N fragment of the adjacent DCA molecule. This leaves isolated N–C $\equiv$ N and N–C fragments separated by the "bond-shifted" DCA molecule. This "bond-breaking" (BB) model was found stable even up
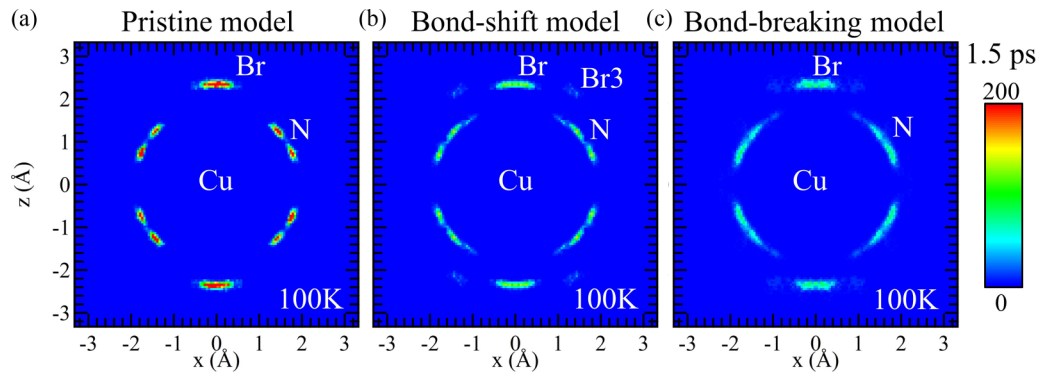
FIG. 6. 2D histograms of the relative positions of the nearest neighboring Br and N atoms at 100 K obtained from the 1.5-ps molecular dynamics simulations of the (a) pristine model, (b) bond-shift model and (c) the bond-breaking model.

to 300 K. The isolated fragments are marked by the red circles in Fig. 5(f), while the single "bond-shifted" DCA molecule is marked by a dashed square.

Figure 5(d) shows the reconstruction of the anion layer, where both the Br and N atoms are clearly observed. Compared to the reconstruction obtained from the simulations of the BS model in Fig. 5(c), no atomic images are observed at the Br3 site. This is due to the low concentration of Br3 atoms in the BB model, where only one bond-shifted DCA molecule is introduced in the anion layer. The defect concentration of this model is so low that the resulting reconstructed anion layer is almost identical to the reconstruction from the pristine model in Fig. 4(b).

In all the simulations considered so far, the N atomic images are consistently much stronger than was observed in the experiment for the irradiated samples. This suggests that the static displacements in the structural models are not enough to suppress the N atomic images. The XFH simulations presented so far does not include any thermal vibrations, thus, the suppression of the N atomic images in the experiment is most likely due to dynamic fluctuations of the N atoms due to thermal vibration. In the next section, these dynamic fluctuations are investigated using MD simulations and additional XFH simulations.

C. Simulations: Molecular dynamics and x-ray fluorescence holography

To investigate the effects of dynamic fluctuations on the simulated holograms, MD simulations were performed on the pristine, "bond-shift" and "bond-breaking" models. For these structural models, 150 snapshots every 10 fs were extracted from the MD trajectories at 100 and 300 K. From the atomic positions at each frame, the positions of the scatterers relative to the Cu emitter were extracted. The calculated relative positions now include both the static and dynamic displacements of the atoms. Figure 6 shows the 2D histograms of the positions of the nearest neighboring Br and N atoms of the three structural models at 100 K. For the pristine model [Fig. 6(a)], the distribution of both Br and N atoms are sharp, centered on the Br and N positions of the pristine model in Fig. 4(c). For both the BS and BB models, the positional distributions of the Br and N atoms are broadened along the angular direction, with an additional distribution for the Br3 atoms in the bond-shift model.

The effects of the positional fluctuation of the scatterers on the reconstructed atomic image has been systematically studied by some of the authors of this work in Ref. [15]. Hayashi *et al.* [15], simulated the holograms of a simple Zn–Te dimer system and found that by introducing a disklike or a spherical distribution in the position of the Te scatterer, the intensity of the reconstructed image can be significantly suppressed. While a spherical positional distribution is more analogous to thermal vibrations of atoms, the disklike distribution is a more appropriate approximation in situations where the emitter-scatterer bond length is fixed and that the only degree of freedom is along the angular direction [34]. In this case, the angular direction can be approximated as perpendicular to the radial direction, giving a disklike distribution (inset of Fig. 7). From the disklike distribution in the Zn–Te dimer system, a standard deviation value (σ_A) of 0.2 Å in the scatterer position results in the suppression of the Te atomic image intensity to 60% of the ideal system [15].

From the atomic positions calculated for 1.5 ps in the MD simulations, the standard deviations of the relative positions of the nearest neighboring Br and N atoms were calculated
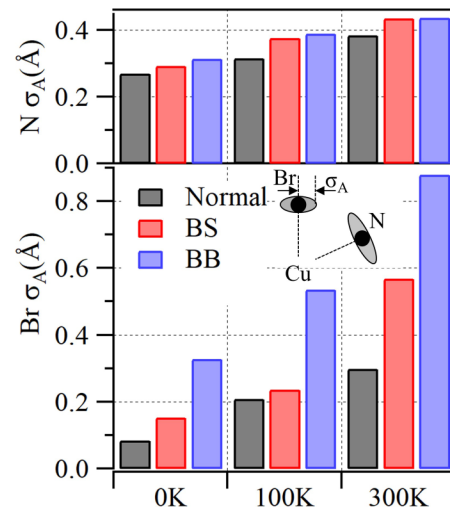

FIG. 7. The standard deviations of the angular positional distributions of the nearest neighboring Br and N atoms in the normal, bond-shift and bond-breaking models after 1.5-ps molecular dynamics simulations at 0, 100, and 300 K.

along the angular (σ_A) direction and are summarized in Fig. 7. The 0 K distributions represent the static distribution of the scatterers relative to the Cu atoms and were used in the XFH simulations and their corresponding reconstructions in Figs. 4(b), 5(c), and 5(d). For the σ_A calculations for Br atoms at 0 and 100 K, the values for the Br atoms at the Br3 sites were excluded as the simulation in Fig. 5(c) showed that this results in a separate Br atomic image in the reconstruction. At 300 K, the large thermal fluctuations vibrations make the Br and Br3 atoms indistinguishable.

At 0 K the introduction of the bond-shift defects in the BS model results in a large increase in the positional fluctuations in the Br atoms, almost doubling the σ_A value of the BS model compared to the normal model at 0 K. For N, there is an inherently larger static fluctuation as a result of the complicated local structure around Cu. This is from the superposition of the different local structures, as was shown in Fig. 1(c).

At higher temperatures, the σ_A values for both Br and N atoms increase for all models, consistent with thermal vibrations. For N at 100 K, the σ_A value of the BS model is $\sim$0.1Å higher than the normal model, which will result in a suppression of the N atomic image intensity by 20% [15].

For the BB model, the large σ_A values for Br are inconsistent with the strong Br atomic image intensities experimentally observed for the irradiated samples [Figs. 5(a) and 5(b)]. Furthermore, the σ_A values of both Br and N atoms in the BB model are higher than the BS model despite the BB model only having a single bond-shifted DCA molecule. This suggests that the isolated DCA fragments could be introducing strong instabilities in the DCA network that results in the large σ values.

To isolate how the σ_A values can affect the atomic images in the reconstruction, a series of simple hologram simulations were done using only Cu and N atoms, beginning with an ideal Cu–N dimer system, whose reconstruction is shown in Fig. 8(a). In this ideal dimer system, the N atom is placed in the average N position of the pristine κ-Br model, as indicated by the red circle.

In Figs. 8(b)–8(d), a series of XFH simulations and atomic reconstructions were made using the distribution of N atoms in the pristine κ-Br model, BS and BB models at 0 K. With increasing σ_A values, the shape of the N atomic images hardly changed, but the intensities are suppressed. The suppression of the intensities, relative to the ideal Cu-N dimer system is summarized in Fig. 8(e). At 0 and 100 K, the N atomic image intensities of the BS model is 11% and 9% lower than the pristine κ-Br. While this trend is consistent with what is observed in the experiments, the $\sim$10% suppression in this simulation is less than the atomic image intensity suppression observed in the irradiated samples.

Since the x-ray fluorescence holographic signal, and the resulting reconstruction, consists of the sum of holographic oscillations from all the scatterers around the Cu emitter atoms, another set of holograms were simulated using a 5 Å radius cluster around Cu constructed from the relative positions of all scatterers calculated from the 1.5-ps MD simulations at 100 K.

The atomic image reconstructed from the hologram simulations of the pristine model at 100 K [Fig. 9(a)] agrees well with the reconstruction from the pristine sample in Fig. 4(a),
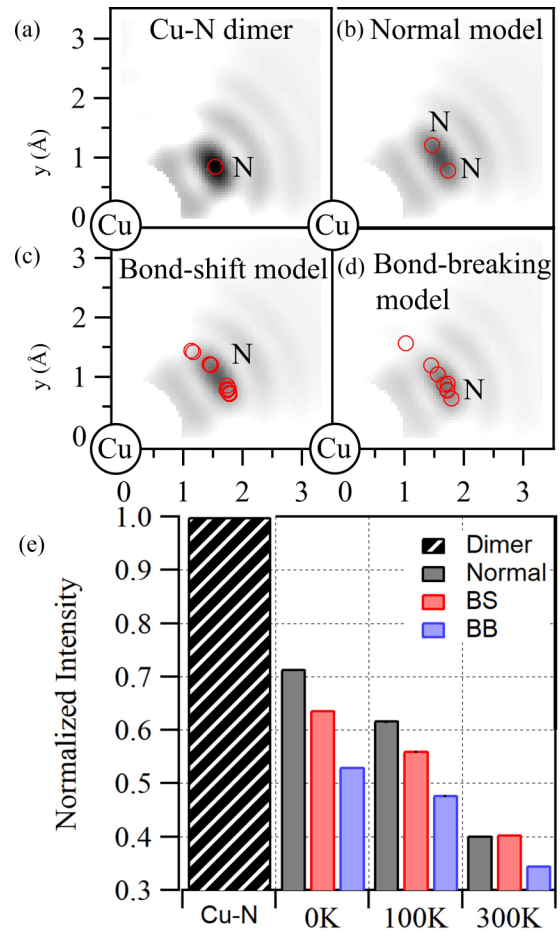

FIG. 8. Atomic reconstructions from the holograms simulated at 0 K from (a) a simple Cu-N dimer system and the Cu and N atoms only from (b) the pristine κ-Br model, (c) the bond-shift model and the (d) the bond-breaking model. (e) Summary of the normalized N atomic image intensities from the simulations at different temperatures.

with strong Br atomic images and weak N images. For the BS and BB models, the effects on the Br atomic images are minimal while the N atomic images are strongly suppressed and are barely visible above the background noise levels [Figs. 9(b) and 9(c)]. In particular, in the BS model, the N atomic images are reduced by 15% when compared to the pristine model.

These simulations show that the increased static positional fluctuations introduced by the bond-shift defects in the BS model, and the dynamic fluctuations due to thermal vibrations at 100 K can strongly suppress the N atomic images, which agrees well with the results of the experiment. This suggests that the defect formation in κ-Br follows the double-excitation process which leads to a bond-shifted structure (the BS model) as predicted in DFT calculations [7].

It should be noted that while the XFH simulations of the BS model at 100 K resulted in the suppression of the N atomic image intensity that is consistent with the experiment, the amount of suppression is only $\sim$15% from the pristine model. In the experiment, the N atomic images of the irradiated samples are strongly suppressed and are no longer visible in the reconstruction. Several scenarios are considered
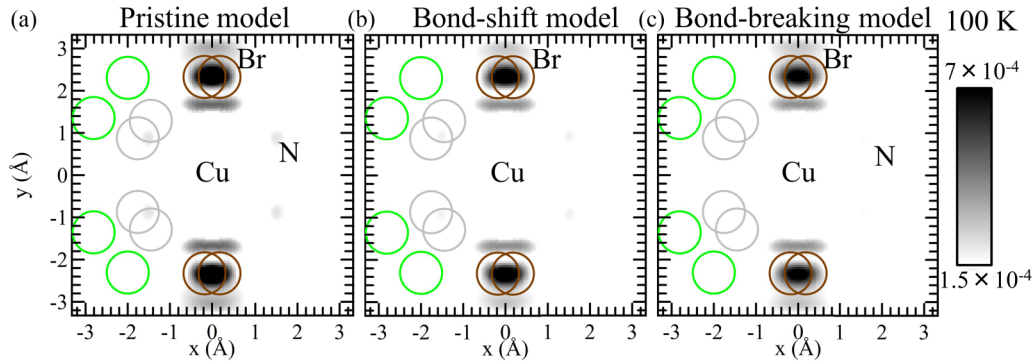
FIG. 9. Reconstruction of the anion layer from holograms simulated at 100 K using the MD simulation results for the (a) pristine model, (b) the bond-shift model and (c) the bond-breaking model.

that may explain the inconsistencies in the N atomic image suppression between the experiment and the BS model simulations.

First, this is probably due to an underestimation of the thermal vibration amplitudes in the MD simulations of the BS model. For the pristine κ-Br model, which was based on experimental diffraction results, the agreement between the XFH simulations at 100 K and the experiment shows that the thermal vibration amplitudes obtained in the MD simulations are close to the actual values. For the irradiated samples, the suppression of the N atomic images behaves more like the 300-K simulations in Fig. 8(c), suggesting that the thermal vibrations in the irradiated samples are greater than which is predicted by the MD simulations. For such a scenario, the Br atomic images in the irradiated samples should similarly be affected. This is, however, not the case in the experimental reconstructions, where the intensity of the Br atomic images is almost constant even after irradiation. As discussed in the previous section, this is due to the large displacement of the Br atoms in the bond-shifted region [Br3 in Fig. 5(c)], where the there is only a small broadening of the Br distribution in the non-bond-shifted regions of the irradiated sample. Furthermore, it has been suggested that a glasslike transition observed in κ-Br and κ-(BEDT-TTF)$_2$Cu[N(CN)$_2$]Cl results in the freezing out of the collective motion of the ethylene end groups (EEGs) of the BEDT-TTF molecules and the terminal ligands (Z = Br- or Cl-) below the glass transition temperature T_g [35]. The strong vdW coupling between the EEGs and the anion layers are dominated by Z···H contacts between the EEGs and the terminal ligands. This results in the coupling of the EEG rotation with the in-plane motion of these terminal ligands, both of which freeze out at T_g. The glass transition temperature $T_g \approx 70$ K has been reported from various thermodynamic measurements [35–38], and x-ray diffraction [19,39]. This transition temperature T_g shifts to higher temperatures with increasing cooling rates [36]. This may explain why the Br atomic images are not as affected by the thermal vibrations at 100 K.

Another possible scenario is the randomness of the defects in the actual irradiated samples. In the formation of the BS model, 2 N atoms from adjacent DCA molecules are excited by the x-ray irradiation and leads to C–N bond breaking. The broken N–C≡N and C≡N fragments from adjacent DCA- fragments connect thru thermal motion and form the

bond-shifted DCA molecule. Further reactions proceed from the remaining DCA- fragments and eventually an alignment of these bond-shifted DCA molecules along the c direction is formed. This results in periodic defects. However, in our simulations, the introduction of random defects results in the fragmentation of the DCA network upon structural optimizations. To realize such a random distribution of defects, additional simulations of structures not considered in this work might be necessary.

While additional experiments can further clarify this situation, the XFH experiment, the XFH simulations, and the MD simulations done in this work provide experimental evidence that the radiation damage in κ-Br results in permanent deformation in accordance with the "bond-shift" model. Atomic reconstructions show a strong suppression of N atomic images due to increased positional fluctuations of the N atoms after inducing radiation damage. By including the thermal motion of atoms in the clusters used in the XFH simulations, the resulting reconstruction of anion plane that agrees well with the experimental results. Furthermore, these results show the successful application of XFH on molecular crystals, opening up the possibility of future investigations of soft materials using this element sensitive, atomic resolution technique.

IV. CONCLUSIONS

X-ray fluorescence holography experiments were performed on pristine and irradiated κ-(BEDT-TTF)$_2$Cu[N(CN)$_2$]Br crystals to investigate the effects of irradiation on the local structures around Cu in the anion layer as the sample goes through a metal-insulator transition. The atomic reconstruction of the anion layer of the pristine κ-Br crystal clearly shows the nearest neighboring Br and N atomic images, showing similarities with the reconstructions obtained from simulated holograms.

After x-ray irradiation, permanent deformation is introduced in κ-Br and this was reflected in the suppression of the N atomic images in the reconstructions. Using the "bond-shifted" model, and molecular dynamics simulations, the combined static and dynamic fluctuations in the atomic positions around Cu in the anion layer were introduced in the hologram simulations. The reconstructions from the pristine and BS model at 100 K better reproduces the experimental reconstructions, showing that the static fluctuations from the BS

model, and the dynamic (thermal vibrations) fluctuations can sufficiently suppress the N atomic images, as was observed experimentally. The results of the XFH experiments provide experimental evidence that the BS model is a good model of the permanent deformation induced in κ-Br upon x-ray irradiation. These results provide key structural information that can help us understand how x-ray irradiation leads to the metal-insulator transition in this series of strongly correlated electron systems. Furthermore, the clear atomic reconstructions obtained from the XFH experiments demonstrates that XFH can be a powerful tool in examining the local structure around metals in organic samples, opening up the possibility of future bio-XFH experiments.

[1] B. J. Powell and R. H. McKenzie, J. Phys. Condens. Matter **18**, R827 (2006).

[2] J. G. Analytis, A. Ardavan, S. J. Blundell, R. L. Owen, E. F. Garman, C. Jeynes, and B. J. Powell, Phys. Rev. Lett. **96**, 177002 (2006).

[3] T. Sasaki, H. Oizumi, N. Yoneyama, N. Kobayashi, and N. Toyota, J. Phys. Soc. Jpn. **76**, 123701 (2007).

[4] K. Sano, T. Sasaki, N. Yoneyama, and N. Kobayashi, Phys. Rev. Lett. **104**, 217003 (2010).

[5] T. Sasaki, K. Sano, H. Sugawara, N. Yoneyama, and N. Kobayashi, Phys. Status Solidi B **249**, 947 (2012).

[6] T. Sasaki, Crystals **2**, 374 (2012).

[7] L. Kang, K. Akagi, K. Hayashi, and T. Sasaki, Phys. Rev. B **95**, 214106 (2017).

[8] G. Faigel and M. Tegze, Rep. Prog. Phys. **62**, 355 (1999).

[9] K. Hayashi, N. Happo, S. Hosokawa, W. Hu, and T. Matsushita, J. Phys.: Condens. Matter **24**, 093201 (2012).

[10] T. Yamamoto, K. Hayashi, N. Happo, S. Hosokawa, and H. Tajiri, Acta Mater. **131**, 534 (2017).

[11] S. Hosokawa, J. R. Stellhorn, T. Matsushita, N. Happo, K. Kimura, K. Hayashi, Y. Ebisu, T. Ozaki, H. Ikemoto, H. Setoyama, T. Okajima, Y. Yoda, H. Ishii, Y. F. Liao, M. Kitaura, and M. Sasaki, Phys. Rev. B **96**, 214207 (2017).

[12] K. Kimura, K. Hayashi, L. V. Yashina, N. Happo, T. Nishioka, Y. Yamamoto, Y. Ebisu, T. Ozaki, S. Hosokawa, T. Matsushita, and H. Tajiri, Surf. Interface Anal. **51**, 51 (2019).

[13] T. Sekioka, K. Hayashi, E. Matsubara, Y. Takahashi, T. Hayashi, M. Terasawa, T. Mitamura, A. Iwase, and O. Michikami, J. Synchrotron Radiat. **12**, 530 (2005).

[14] K. Hayashi, N. Uchitomi, K. Yamagami, A. Suzuki, H. Yoshizawa, J. T. Asubar, N. Happo, and S. Hosokawa, J. Appl. Phys. **119**, 125703 (2016).

[15] K. Hayashi, N. Happo, and S. Hosokawa, J. Electron Spectros. Relat. Phenomena **195**, 337 (2014).

[16] K. Hayashi and P. Korecki, J. Phys. Soc. Jpn. **87**, 061003 (2018).

[17] A. Sato-Tomita, N. Shibayama, N. Happo, K. Kimura, T. Okabe, T. Matsushita, S. Y. Park, Y. C. Sasaki, and K. Hayashi, Rev. Sci. Instrum. **87**, 063707 (2016).

[18] A. K. R. Ang, A. Sato-Tomita, N. Shibayama, Y. Umena, N. Happo, R. Marumi, K. Kimura, T. Matsushita, K. Akagi, T. Sasaki, Y. C. Sasaki, and K. Hayashi, Jpn. J. Appl. Phys. **59**, 010505 (2020).

[19] A. U. B. Wolter, R. Feyerherm, E. Dudzik, S. Süllow, C. Strack, M. Lang, and D. Schweitzer, Phys. Rev. B **75**, 104512 (2007).

[20] See Supplemental Materials at http://link.aps.org/supplemental/10.1103/PhysRevB.103.214106 for details about the evaluation of radiation damage and the interpretation of the atomic images in the reconstruction.

[21] O. B. Zeldin, M. Gerstel, and E. F. Garman, J. Appl. Crystallogr. **46**, 1225 (2013).

[22] J. J. Barton, Phys. Rev. Lett. **67**, 3106 (1991).

[23] G. Kresse and J. Hafner, Phys. Rev. B **47**, 558 (1993).

[24] I. Hamada, Phys. Rev. B **89**, 121103(R) (2014).

[25] W. Kossel, V. Loeck, and H. Voegs, Z. Phys. **94**, 139 (1935).

[26] G. Bortel, G. Faigel, M. Tegze, and A. Chumakov, J. Synchrotron Radiat. **23**, 214 (2016).

[27] A. M. Kini, U. Geiser, H. H. Wang, K. D. Carlson, J. M. Williams, W. K. Kwok, K. G. Vandervoort, J. E. Thompson, D. L. Stupka, D. Jung, and M. H. Whangbo, Inorg. Chem. **29**, 2555 (1990).

[28] U. Geiser, A. J. Schults, H. H. Wang, D. M. Watkins, D. L. Stupka, J. M. Williams, J. E. Schirber, D. L. Overmyer, D. Jung, J. J. Novoa, and M. H. Whangbo, Phys. C **174**, 475 (1991).

[29] T. Doi, K. Oshima, H. Maeda, H. Yamazaki, H. Maruyama, K. Kimura, M. Fujita, H. Mori, S. Tanaka, H. Yamochi, and G. Saito, Phys. C **185–189**, 2671 (1991).

[30] W. Hu, K. Hayashi, K. Ohwada, J. Chen, N. Happo, S. Hosokawa, M. Takahasi, A. A. Bokov, and Z. G. Ye, Phys. Rev. B **89**, 140103(R) (2014).

[31] J. R. Stellhorn, S. Hosokawa, N. Happo, H. Tajiri, T. Matsushita, K. Kaminaga, T. Fukumura, T. Hasegawa, and K. Hayashi, J. Appl. Crystallogr. **50**, 1583 (2017).

[32] C. Strack, C. Akinci, V. Pashchenko, B. Wolf, E. Uhrig, W. Assmus, M. Lang, J. Schreuer, L. Wiehl, J. A. Schlueter, J. Wosnitza, D. Schweitzer, J. Müller, and J. Wykhoff, Phys. Rev. B **72**, 054511 (2005).

[33] K. Kimura, K. Yokochi, R. Kondo, D. Urushihara, Y. Yamamoto, A. K. R. Ang, N. Happo, K. Ohara, T. Matsushita, T. Asaka, M. Iwata, and K. Hayashi, Jpn. J. Appl. Phys. **58**, 100601 (2019).

[34] S. Hosokawa, N. Happo, T. Ozaki, H. Ikemoto, T. Shishido, and K. Hayashi, Phys. Rev. B **87**, 094104 (2013).

[35] J. Müller, B. Hartmann, R. Rommel, J. Brandenburg, S. M. Winter, and J. A. Schlueter, New J. Phys. **17**, 83057 (2015).

[36] J. Müller, M. Lang, F. Steglich, J. A. Schlueter, A. M. Kini, and T. Sasaki, Phys. Rev. B **65**, 144521 (2002).

[37] H. Akutsu, K. Saito, and M. Sorai, Phys. Rev. B **61**, 4346 (2000).

[38] M. Kund, H. Müller, W. Biberacher, and K. Andres, Phys. B **191**, 274 (1993).

[39] Y. Watanabe, H. Sato, T. Sasaki, and N. Toyota, J. Phys. Soc. Jpn. **60**, 3608 (1991).